

Synthesis and Electrocatalytic Activity of Au–Pd Alloy Nanodendrites for Ethanol Oxidation

Young Wook Lee,^{†,‡} Minjung Kim,^{†,‡} Yena Kim,[‡] Shin Wook Kang,[†] Joon-Hwa Lee,[‡] and Sang Woo Han^{*,†}

Department of Chemistry and KI for the NanoCentury, KAIST, Daejeon 305-701, Korea, and Department of Chemistry, Research Institute of Natural Science, and Environmental Biotechnology National Core Research Center, Gyeongsang National University, Jinju 660-701, Korea

Received: December 18, 2009; Revised Manuscript Received: March 29, 2010

Dendritic Au–Pd alloy nanoparticles were synthesized in high yield through the coreduction of HAuCl₄ and K₂PdCl₄ in aqueous solutions by using hydrazine as a reducing agent. Relative compositions between Au and Pd at the particle surfaces as well as in bulk phases could be modulated by controlling the molar ratios between metal precursors in the feeding solutions. The formation of nanodendrites may be the result of the fast reduction rate of metal ions and subsequent fast, kinetically controlled growth of particles. The prepared alloy nanoparticles exhibit efficient electrocatalytic activities and stabilities toward ethanol oxidation in alkaline media. The enhanced electrocatalytic properties of dendritic particles can be attributed to the presence of a large number of active sites on their surfaces.

1. Introduction

Bimetallic nanoparticles with core–shell or alloy structures are an attractive target of catalytic research due to their enhanced properties, such as selectivity, activity, and chemical/physical stability, being distinct from those of the corresponding monometallic components.¹ Specifically, large efforts are being directed toward the synthesis of alloy nanocatalysts for the application in direct alcohol fuel cells because alloy nanoparticles often exhibit higher electrocatalytic activities toward methanol or ethanol oxidation than monometallic particles.² The catalytic properties of bimetallic nanoparticles can be changed by tuning the chemical composition and also be modulated by controlling their size and shape, as in the case of monometallic nanoparticles. Accordingly, rationally designed bimetallic nanoparticles with controlled morphology may show optimized properties.^{3,4}

Among the various bimetallic nanoparticles, Au–Pd alloy nanoparticles have been widely explored as catalytic materials for a variety of reactions.⁵ Recently, it has been shown that the Au–Pd nanocatalysts give enhanced electrocatalytic activity for the oxidation of alcohols.⁶ Although a number of reports have focused on the preparation and characterization of Au–Pd alloy nanoparticles, the synthesis of particles with unconventional shapes and controlled atomic distribution remains relatively unexplored. Very recently, we have reported an aqueous-phase synthesis of flower-shaped porous Au–Pd alloy nanoparticles through the coreduction of Au and Pd ions with ascorbic acid as a reductant.⁷ The bulk compositions of alloy nanoparticles were roughly consistent with those of the feeding solutions. However, the surface compositions of prepared particles significantly deviate from the bulk values; all alloy nanoparticles have Pd-enriched surfaces. Because the catalytic effects of nanoparticles are strongly influenced by the structure and

composition of their surfaces, fine-structuring of the outermost layers of catalytic nanoparticles is a very critical issue in the applications.⁸

In this paper, we describe a facile aqueous-phase method to synthesize dendritic Au–Pd alloy nanoparticles. Alloy nanodendrites were readily formed upon the coreduction of HAuCl₄ and K₂PdCl₄ by a strong reductant, that is, hydrazine, in aqueous solution. Because of its high reducing power, hydrazine could accelerate the reduction kinetics of metal precursors, resulting in the formation of the particles with such an unusual shape.⁹ Furthermore, relative molar ratios between Au and Pd at the particle surfaces as well as in bulk phases could be controlled by adjusting the molar ratios between metal precursors in the feeding solutions. Because dendritic structures have exhibited relatively large surface areas and highly active facets on their surfaces,^{4,10} it can be expected that the prepared particles may show enhanced catalytic efficiencies. In this regard, we have also investigated the electrocatalytic activities of the synthesized nanoparticles toward ethanol oxidation.

2. Experimental Section

2.1. Chemicals and Materials. HAuCl₄ (Aldrich, 99.99+%), K₂PdCl₄ (Aldrich, 99.99%), hydrazine hydrate (N₂H₄·H₂O, Aldrich, 64%), and poly(vinyl pyrrolidone) (PVP, *M_w* ≈ 55 000) were all used as received. Other chemicals, unless specified, were reagent grade, and Milli-Q water with a resistivity of greater than 18.0 MΩ·cm was used in the preparation of aqueous solutions.

2.2. Preparation of Nanoparticles. In a typical synthesis of Au–Pd bimetallic nanoparticles, 1 mL of a 5 mM aqueous solution of HAuCl₄/K₂PdCl₄ mixtures in molar ratios of 3/1, 1/1, and 1/3 was added to 47 mL of highly purified water. To this solution was added 1 mL of 100 mM hydrazine. After 15 s, an aqueous solution of PVP (5 mg/mL, 1 mL) was added dropwise with vigorous stirring, and the solution was stirred further for 5 min. The resultant hydrosol was subjected to centrifugation (10 000 rpm for 5 min) to remove excess reagent. For comparison, Au and Pd monometallic nanoparticles were prepared

* To whom correspondence should be addressed. E-mail: sangwoohan@kaist.ac.kr.

† KAIST.

‡ Gyeongsang National University.

in the same way by substituting an aqueous solution of HAuCl₄/K₂PdCl₄ mixtures with HAuCl₄ and K₂PdCl₄ solutions, respectively.

2.3. Characterization of Nanoparticles. The extinction spectra were recorded with a UV-vis absorption spectrometer (SINCO S-3100). Transmission electron microscopy (TEM) images and energy-dispersive X-ray spectroscopy (EDS) data were obtained with a JEOL JEM-2010 transmission electron microscope operating at 200 kV after placing a drop of hydrosol on carbon-coated Cu grids (200 mesh). High-resolution TEM (HRTEM) characterizations were performed with a FEI Technai G2 F30 Super-Twin transmission electron microscope operating at 300 kV. Indium-tin oxide (ITO) was used as the substrate for X-ray diffraction (XRD) and cyclic voltammetry (CV) measurements. The ITO substrate was chosen for the convenience of sample preparation; cleaning and deposition of nanoparticles could be easily performed with ITO substrates.¹¹ The ITO substrate was washed with sonication in acetone and then pure water. The washed ITO substrates were dried in the air and then immersed in a 2-propanol solution of 1% 3-amino-propyltrimethoxysilane for 3 h, yielding an amine-terminated surface.¹² The modified substrates were rinsed thoroughly with pure water prior to use. For immobilization of nanoparticles, 0.1 mL of hydrosol was dropped onto the amine-terminated ITO substrates and dried under ambient condition. The substrate was then washed with water and dried. XRD patterns were obtained with a Bruker AXS D8 DISCOVER diffractometer using Cu K α (0.1542 nm) radiation. CV measurements were carried out in a three-electrode cell using a CH Instrument model 600C potentiostat. Nanoparticle-modified ITO substrates served as working electrodes. Before CV measurements, the nanoparticle-modified substrates were cleaned again by sequentially washing with acetone, ethanol, and water to remove stabilizing agents on the surface of nanoparticles. Pt wire and Ag/AgCl (in saturated KCl) were used as the counter and reference electrodes, respectively. All cyclic voltammograms were obtained at room temperature. The electrolyte solutions were purged with high-purity N₂ gas before use for about 1 h.

3. Results and Discussion

Au-Pd alloy nanodendrites were synthesized by coreduction of HAuCl₄/K₂PdCl₄ mixtures with hydrazine in the presence of PVP. Hereafter, we will refer to the particles prepared from the aqueous solutions of HAuCl₄/K₂PdCl₄ mixtures in molar ratios of 3/1, 1/1, and 1/3 as Au₃Pd₁, Au₁Pd₁, and Au₁Pd₃, respectively. Figure 1a shows a representative TEM image of the prepared Au₁Pd₁ sample, which demonstrates that the synthesized particles have a dendritic structure with a number of branches. The average circular diameter of the dendritic nanoparticles obtained by measuring the length from a branch edge to another one on the opposite side was 21 ± 5 nm. Au₃Pd₁ and Au₁Pd₃ samples also have dendritic shapes, and the measured average sizes are 26 ± 5 and 15 ± 2 nm, respectively (Figure 1b,c). We further analyzed the Au-Pd nanodendrites by using HRTEM. Figure 2a shows a typical HRTEM image of a dendritic nanoparticle, which shows that the prepared particles have a good crystalline structure with well-defined lattice fringes. The *d* spacing for adjacent lattice fringes measured from several different points on a single nanoparticle was 2.30 Å (Figure 2b), which corresponds to the mean value of the (111) planes of face-centered cubic (fcc) Au and Pd,⁷ indicating that most of the exposed facets of the Au-Pd nanodendrites were {111}.

To further investigate the alloy nature of the prepared nanoparticles, Au-Pd nanodendrites were characterized with

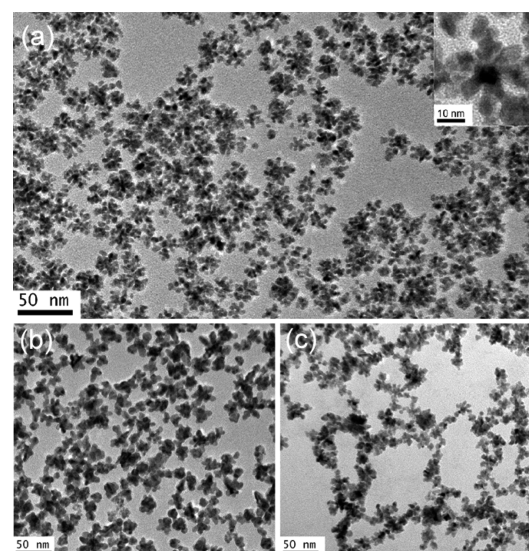


Figure 1. TEM images of (a) Au₁Pd₁, (b) Au₃Pd₁, and (c) Au₁Pd₃ bimetallic nanoparticles. The inset in (a) shows a magnified image.

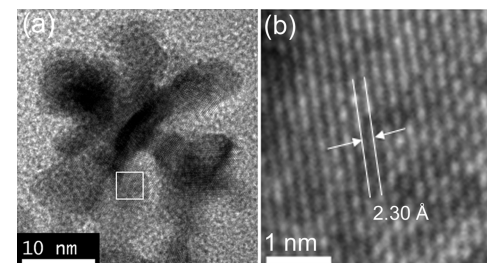


Figure 2. (a) HRTEM image of the Au₁Pd₁ bimetallic nanoparticle. (b) High-magnification HRTEM image of the square region in (a).

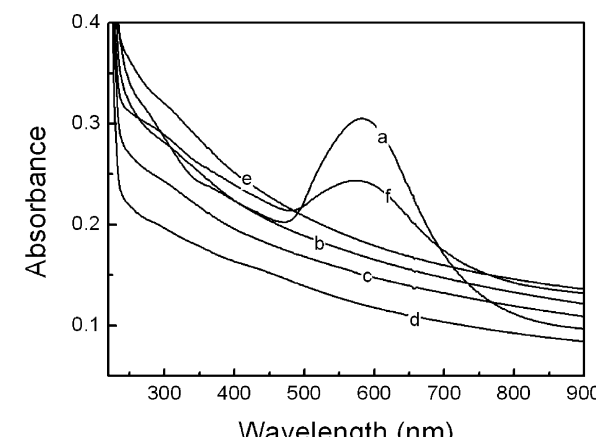


Figure 3. UV-vis absorption spectra of (a) Au, (b) Au₃Pd₁, (c) Au₁Pd₁, (d) Au₁Pd₃, and (e) Pd nanoparticles and a (f) 1:1 physical mixture of Au and Pd nanoparticles.

EDS, UV-vis spectroscopy, and XRD. The mole fractions of Pd in Au₃Pd₁, Au₁Pd₁, and Au₁Pd₃ samples obtained from EDS data were 0.21, 0.45, and 0.66, respectively, indicating that the compositions of nanoparticles were roughly consistent with those of the feeding solutions. The UV-vis spectral features of the Au-Pd nanodendrites were found to be different from those of the individual and physical mixture of the monometallic nanoparticles (Figure 3). This clearly indicates that dispersions of Au-Pd nanoparticle systems do not contain monometallic particles but contain nanoparticles with bimetallic structure. This result coincides with the previous report of Wu et al.¹³ The absence of peaks at 310 and 440/325 nm correspond to

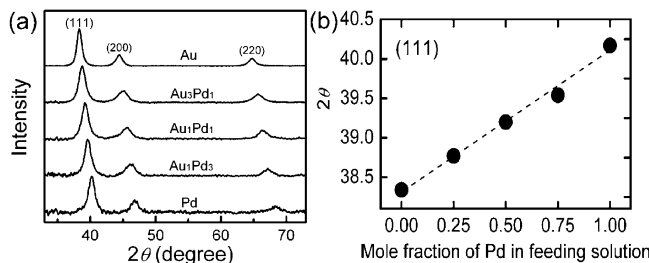


Figure 4. (a) XRD patterns and (b) (111) diffraction peak positions of the Au, Pd, and Au–Pd bimetallic nanoparticles on ITO glasses.

unreduced Au and Pd precursors, respectively and also indicates complete reduction of the metal ions. Figure 4a shows the XRD patterns of Au, Pd, and Au–Pd nanoparticles. Each pattern exhibits three diffraction peaks that can be indexed to diffraction from the (111), (200), and (220) of the fcc structure of metallic Au and/or Pd. The diffraction peaks of the bimetallic particles exhibit a shift from pure Au to pure Pd as the Pd content increases, and a good linear relationship was found between the peak position and mole fraction of Pd in the feeding solution (Figure 4b), suggesting that the prepared nanoparticles were Au–Pd alloys and the composition of each bimetallic nanoparticle was proportional to that of the feeding solution.¹⁴

Although the detailed mechanism for the growth of the dendritic particles is yet to be resolved, the formation of nanodendrites may be the result of the fast reduction rate of metal ions and the corresponding fast nucleation and growth of particles. It has been reported that a high concentration of metallic seeds is crucial for the formation of multibranched nanoparticles.¹⁵ In our experiment, hydrazine was used as a reducing agent. Owing to its high reducing capability, there will be a large amount of reduced metal precursors at the initial stage of reaction,^{15d} and subsequent fast, kinetically controlled growth of nanoparticles resulted in the growth of dendritic particles.¹⁶ Under the thermodynamically controlled reaction conditions, the formation of roughly spherical isotropic particles with a lower surface area than that of dendritic particles was favored to minimize the surface energy.¹⁶ As mentioned previously, flower-like porous structures were formed when the analogue reaction was conducted with the milder reductant, that is, ascorbic acid.⁷ The different reduction kinetics between two reductants can be inferred from the standard reduction potentials of hydrazine (-0.23 V vs SHE (standard hydrogen electrode))¹⁷ and ascorbic acid ($+0.4$ V vs SHE).¹⁸

The surface properties of Au–Pd alloy nanodendrites were characterized by CV measurement. Figure 5a shows a series of cyclic voltammograms (CVs) of ITO electrodes modified with the Au–Pd alloy nanodendrites obtained in 0.1 M KOH at a scan rate of 50 mV s $^{-1}$. CVs obtained from monometallic Au and Pd particles are also shown in Figure 5a for comparison. Typical redox peaks associated with the oxidation/reduction of Au, Pd, and Au–Pd alloy as well as hydrogen adsorption/desorption were observed.¹⁹ The total loading amounts of metal were adjusted to 0.79 mg cm $^{-2}$ for all samples, and the current densities were normalized to the electrochemically active surface areas (ECAS), which were calculated by measuring the Coulombic charge for oxygen desorption.²⁰ The observation of a single oxygen desorption peak with a potential value intervening between those of Au and Pd for all the alloy nanoparticles (-0.08 ± 0.03 , -0.13 ± 0.02 , and -0.18 ± 0.02 V vs Ag/AgCl for Au₃Pd₁, Au₁Pd₁, and Au₁Pd₃, respectively) demonstrates the relatively homogeneous distribution of Au and Pd atoms on the surface of alloy nanoparticles.^{19,21} The gradual

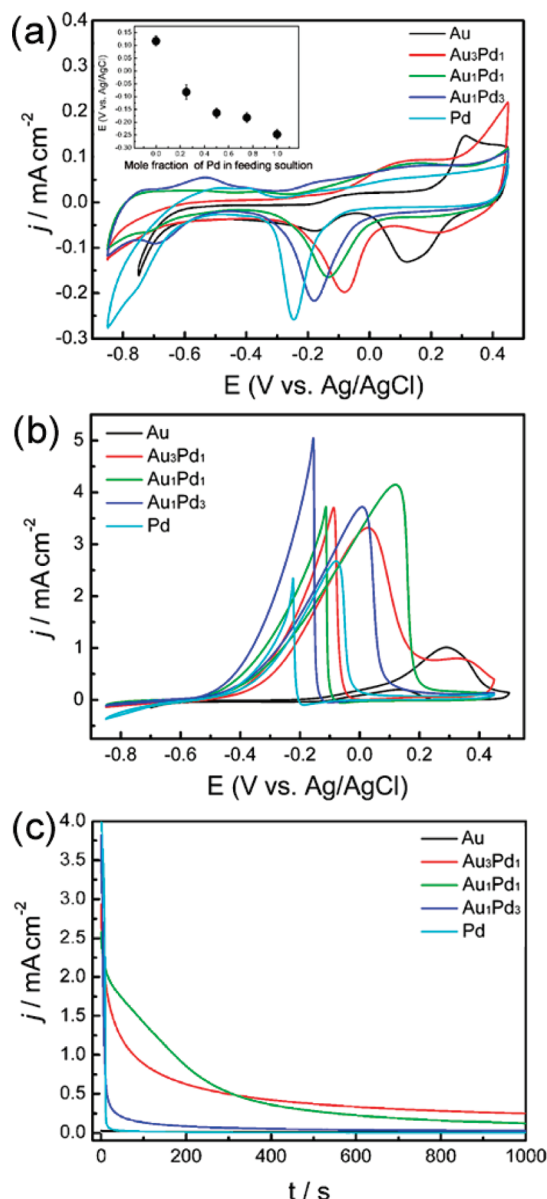


Figure 5. CVs in (a) 0.1 M KOH and (b) 0.1 M KOH + 0.1 M ethanol of Au, Pd, and Au–Pd alloy nanoparticles on ITO electrodes. Scan rate: 50 mV s $^{-1}$. The inset in (a) shows the oxygen desorption peak position of Au, Pd, and Au–Pd alloy nanoparticle-modified ITO electrodes. (c) Chronoamperometric curves for the Au, Pd, and Au–Pd alloy nanoparticles on ITO electrodes in 0.1 M KOH + 0.1 M ethanol at 0.0 V vs Ag/AgCl.

shift of the oxygen desorption peak from pure Au to pure Pd as the Pd content increases also suggests that the surface composition of each bimetallic nanoparticle is proportional to that of the feeding solution (see the inset of Figure 5a).¹⁹ On the contrary, Pd/Au molar ratios at the particle surfaces were higher than 0.8 , regardless of their bulk ratios when using ascorbic acid as a reductant.⁷ Because of the weak reducing power of ascorbic acid, the reduction rate of the metal precursors was slow. On the basis of the reduction potentials of Au (III) and Pd (II) (Au^{3+} (AuCl_4^- /Au, $+1.002$ V vs SHE) and Pd^{2+} (PdCl_4^{2-} /Pd, $+0.591$ V vs SHE)),²² it can be assumed that the formation of the alloy particles should be initiated by nucleation of Au atoms, followed by codeposition of residual Au and Pd atoms on the surface of the seeds that have a higher Au content, resulting in the formation of Pd-enriched surfaces. Very recently, we have found that even Au@Pd core–shell nanoparticles could

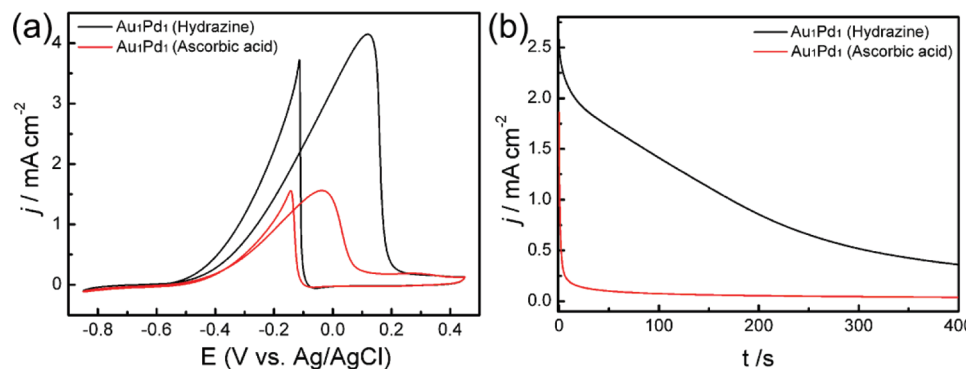


Figure 6. (a) CVs in 0.1 M KOH + 0.1 M ethanol of dendritic and flower-like Au:Pd₁ alloy nanoparticles synthesized by using hydrazine and ascorbic acid, respectively, on ITO electrodes. Scan rate: 50 mV s⁻¹. (b) Chronoamperometric curves for the dendritic and flower-like Au:Pd₁ alloy nanoparticles on ITO electrodes in 0.1 M KOH + 0.1 M ethanol at 0.0 V vs Ag/AgCl.

be formed when Au and Pd precursors are simultaneously reduced by a very weak reducing agent, such as cetyltrimethylammonium chloride.²³ In the present work, we have used hydrazine as the reductant which has a much higher reducing capability than the previous reducing agents, thus facilitating the homogeneous nucleation of Au and Pd precursors during the particle growth. Taken together, our results clearly show that the structure and surface composition of the bimetallic nanoparticles can be readily controlled by the modulation of the reduction kinetics.

To investigate the catalytic activity of Au–Pd nanodendrites, the electrocatalytic properties of the nanodendrites for ethanol oxidation were tested. Although Pt and Pt-based nanocatalysts have been widely studied as electrocatalysts for oxidation of alcohols, non-Pt catalysts, such as Pd-based nanoparticles, have recently been investigated because of the high cost and limited supply of Pt. For instance, Pd has been reported to have a good electrocatalytic activity for ethanol oxidation in alkaline media.²⁴ In fact, the electrocatalytic activity of Pd catalysts toward ethanol oxidation highly depends on the pH of the reaction medium. The oxidation reaction is much faster in alkaline solutions than in acidic solutions because continued dehydrogenation of ethanol cannot readily proceed in acidic medium due to the lack of OH species that can instantly remove hydrogen.²⁵ On the basis of this fact, we have used KOH solutions throughout the electrochemical experiments. Alkaline solution has also been used as a medium for the electrocatalytic oxidation of methanol.²⁶ Figure 5b shows the CVs of ethanol oxidation at Au–Pd alloy nanodendrites in 0.1 M KOH solution containing 0.1 M ethanol at a scan rate of 50 mV s⁻¹. For comparison, the CVs of the monometallic Au and Pd are also shown in Figure 5b. The current densities are normalized with respect to the ECAS. Characteristic well-separated anodic peaks in the forward and reverse sweeps associated with ethanol oxidation were observed. The peak current densities are 3.33, 4.18, 3.74, 2.69, and 1.04 mA cm⁻² for the reactions on the Au₃Pd₁, Au₁Pd₁, Au₁Pd₃, Pd, and Au nanoparticles, respectively. The anodic peak currents on alloy nanoparticles are higher than that on the monometallic Pd nanoparticles. The differences in the current densities between samples cannot be due to the different surface areas because the current values were normalized with respect to the ECSA. The enhanced electrocatalytic activities of the Au–Pd alloy nanoparticles can be attributed to the promotional effect of Au on Pd catalytic activity. It has been well-known that the incorporation of Au into Pd catalysts can improve catalytic activity and selectivity as well as the resistance to poisoning.^{5,6a,27} The electrochemical stabilities of the Au–Pd alloy nanodendrites for ethanol electrooxidation were also investigated by chrono-

amperometric experiments at 0.0 V versus Ag/AgCl (Figure 5c). It is noticeable that the current decays associated with the poisoning of the intermediate species on the Au₃Pd₁ and Au₁Pd₁ nanodendrites are much slower than that on the monometallic Pd nanoparticles, indicating that incorporation of Au into Pd catalysts can enhance not only the electrocatalytic activity but also the electrocatalytic stability toward ethanol oxidation. The Au₁Pd₃ nanodendrites exhibit a lower electrocatalytic stability than that of other nanodendrites due to the relatively smaller amount of Au than other alloy particles. Furthermore, comparison between dendritic Au–Pd nanoparticles and flower-like Au–Pd nanoparticles prepared with ascorbic acid as a reductant reveals that Au–Pd nanodendrites have a higher electrocatalytic activity and stability for ethanol oxidation (Figure 6). These enhanced electrocatalytic properties of dendritic particles may be attributed to the presence of a large number of active sites for the adsorption of active oxygen atoms, which can readily oxidize the intermediates on the nanocatalysts.²⁸ As shown in Figures 5 and 6, a more pronounced electrocatalytic activity can be induced by changing the structure of nanocatalysts, indicating that the structural effect plays a more dominant role in enhancing the catalytic performance than the promotional effect of Au.

4. Conclusions

In summary, we have presented an aqueous room-temperature synthesis method for the preparation of Au–Pd alloy nanodendrites. The surface compositions as well as bulk compositions of each bimetallic nanoparticle are proportional to those of the feeding solution. The fast reduction kinetics due to the high reducing capability of hydrazine plays a crucial role in the formation of dendritic particles with controlled compositions. The dendritic nanoparticles show enhanced electrocatalytic properties toward ethanol oxidation. Because the synthesized nanoparticles have unique structural and catalytic properties, they will find applications in the fabrication of novel nanostructures and direct ethanol fuel cells.

Acknowledgment. This work was supported by the Basic Science Research Program (Grant Nos. KRF-2008-313-C00415, R15-2003-012-01001-0, and R11-2008-052-02003), the Nano R&D Program (Grant No. 2009-0082640), and the Pioneer Research Center Program (Grant No. 2009-0082813) through the National Research Foundation of Korea (NRF) funded by the Korean government (MEST).

References and Notes

- (1) Toshima, N.; Yonezawa, T. *New J. Chem.* **1998**, 22, 1179.

- (2) (a) Xu, D.; Liu, Z.; Yang, H.; Liu, Q.; Zhang, J.; Fang, J.; Zou, S.; Sun, K. *Angew. Chem., Int. Ed.* **2009**, *48*, 4217. (b) Wei, Y.-C.; Liu, C.-W.; Wang, K.-W. *ChemPhysChem* **2009**, *10*, 1230. (c) Wang, Z.-C.; Ma, Z.-M.; Li, H.-L. *Appl. Surf. Sci.* **2008**, *254*, 6521. (d) Gupta, S. S.; Datta, J. *J. Power Sources* **2005**, *145*, 124. (e) Yajima, T.; Uchida, H.; Watanabe, M. *J. Phys. Chem. B* **2004**, *108*, 2654.
- (3) (a) Habas, S. E.; Lee, H.; Radmilovic, V.; Somorjai, G. A.; Yang, P. *Nat. Mater.* **2007**, *6*, 692. (b) Kim, M.; Lee, K. Y.; Jeong, G. H.; Jang, J.; Han, S. W. *Chem. Lett.* **2007**, *36*, 1350.
- (4) (a) Lim, B.; Jiang, M.; Camargo, P. H. C.; Cho, E. C.; Tao, J.; Lu, X.; Xia, Y. *Science* **2009**, *324*, 1302. (b) Peng, Z.; Yang, H. *J. Am. Chem. Soc.* **2009**, *131*, 7542.
- (5) (a) Chen, M.; Kumar, D.; Yi, C.-W.; Goodman, D. W. *Science* **2005**, *310*, 291. (b) Chen, C.-H.; Sarma, L. S.; Chen, J.-M.; Shih, S.-C.; Wang, G.-R.; Liu, D.-G.; Tang, M.-T.; Lee, J.-F.; Hwang, B.-J. *ACS Nano* **2007**, *1*, 114. (c) Enache, D. I.; Edwards, J. K.; Landron, P.; Solsona-Espriu, B.; Carley, A. F.; Herzing, A. A.; Watanabe, M.; Kiely, C. J.; Knight, D. W.; Hutchings, G. J. *Science* **2006**, *311*, 362.
- (6) (a) Ksar, F.; Ramos, L.; Keita, B.; Nadjo, L.; Beaunier, P.; Remita, H. *Chem. Mater.* **2009**, *21*, 3677. (b) Nie, M.; Tang, H.; Wei, Z.; Jiang, S. P.; Shen, P. K. *Electrochem. Commun.* **2007**, *9*, 2375.
- (7) Lee, Y. W.; Kim, N. H.; Lee, K. Y.; Kwon, K.; Kim, M.; Han, S. W. *J. Phys. Chem. C* **2008**, *112*, 6717.
- (8) (a) Tian, N.; Zhou, Z.; Sun, S.; Ding, Y.; Wang, Z. L. *Science* **2007**, *316*, 732. (b) Liu, Z.; Hu, J. E.; Wang, Q.; Gaskell, K.; Frenkel, A. I.; Jackson, G. S.; Eichhorn, B. *J. Am. Chem. Soc.* **2009**, *131*, 6924.
- (9) Jeong, G. H.; Lee, Y. W.; Kim, M.; Han, S. W. *J. Colloid Interface Sci.* **2009**, *329*, 97.
- (10) (a) Wang, L.; Yamauchi, Y. *J. Am. Chem. Soc.* **2009**, *131*, 9152. (b) Wang, L.; Yamauchi, Y. *Chem. Mater.* **2009**, *21*, 3562.
- (11) Lee, Y. W.; Kim, M.; Han, S. W. *Chem. Commun.* **2010**, 1535.
- (12) Xue, C.; Li, Z.; Mirkin, C. A. *Small* **2005**, *1*, 513.
- (13) Wu, M.-L.; Chen, D.-H.; Huang, T.-C. *Langmuir* **2001**, *17*, 3877.
- (14) Damle, C.; Kumar, A.; Sastry, M. *J. Phys. Chem. B* **2002**, *106*, 297.
- (15) (a) Zhong, X.; Feng, Y.; Lieberwirth, I.; Knoll, W. *Chem. Mater.* **2006**, *18*, 2468. (b) Teng, X.; Liang, X.; Maksimuk, S.; Yang, H. *Small* **2006**, *2*, 249. (c) Ren, J.; Tilley, R. D. *Small* **2007**, *3*, 1508. (d) Zhou, P.; Dai, Z.; Fang, M.; Huang, X.; Bao, J.; Gong, J. *J. Phys. Chem. C* **2007**, *111*, 12609.
- (16) (a) Yin, Y.; Alivisatos, P. *Nature* **2005**, *437*, 664. (b) Teng, X.; Yang, H. *Nano Lett.* **2005**, *5*, 885. (c) Watt, J.; Cheong, S.; Toney, M. F.; Ingham, B.; Cookson, J.; Bishop, P. T.; Tilley, R. D. *ACS Nano* **2010**, *4*, 396.
- (17) Park, J. W.; Chae, E. H.; Kim, S. H.; Lee, J. H.; Kim, J. W.; Yoon, S. M.; Choi, J.-Y. *Mater. Chem. Phys.* **2006**, *97*, 371.
- (18) Creutz, C. *Inorg. Chem.* **1981**, *20*, 4449.
- (19) Woods, R. In *Electroanalytical Chemistry: A Series of Advances*; Bard, A. J., Ed.; Marcel Dekker: New York, 1974; Vol. 9, pp 1–162.
- (20) The ECAS was estimated by the following equation, $ECAS = Q_0/q_0$, where Q_0 is the surface charge that can be obtained from the area under the CV trace of oxygen desorption and q_0 is the charge required for desorption of a monolayer of oxygen on the Au–Pd surface (412.5, 417.3, and 419.2 μ C/cm² for the Au₃Pd₁, Au₁Pd₁, and Au₁Pd₃, respectively¹⁹).
- (21) Tominaga, M.; Shimazoe, T.; Nagashima, M.; Kusuda, H.; Kubo, A.; Kuwahara, Y.; Taniguchi, I. *J. Electroanal. Chem.* **2006**, *590*, 37.
- (22) Lee, K. Y.; Kim, M.; Lee, Y. W.; Lee, J.-J.; Han, S. W. *Chem. Phys. Lett.* **2007**, *440*, 249.
- (23) Lee, Y. W.; Kim, M.; Kim, Z. H.; Han, S. W. *J. Am. Chem. Soc.* **2009**, *131*, 17036.
- (24) (a) Shen, P. K.; Xu, C. *Electrochem. Commun.* **2006**, *8*, 184. (b) Wang, H.; Xu, C.; Cheng, F.; Jiang, S. *Electrochem. Commun.* **2007**, *9*, 1212. (c) Xu, C.; Shen, P. K.; Liu, Y. *J. Power Sources* **2007**, *164*, 527. (d) Xu, C.; Wang, H.; Shen, P. K.; Jiang, S. P. *Adv. Mater.* **2007**, *19*, 4256. (e) Tian, N.; Zhou, Z.-Y.; Sun, S.-G. *Chem. Commun.* **2009**, 1502.
- (25) Cui, G.; Song, S.; Shen, P. K.; Kowal, A.; Bianchini, C. *J. Phys. Chem. C* **2009**, *113*, 15639.
- (26) (a) Jena, B. K.; Raj, C. R. *J. Phys. Chem. C* **2007**, *111*, 15146. (b) Jena, B. K.; Raj, C. R. *Langmuir* **2007**, *23*, 4064.
- (27) (a) Venezia, A. M.; La Parola, V.; Deganello, G.; Pawelec, B.; Fierro, J. L. G. *J. Catal.* **2003**, *215*, 317. (b) Atwan, M. H.; Macdonald, C. L. B.; Northwood, D. O.; Gyenge, E. L. *J. Power Sources* **2006**, *158*, 36.
- (28) (a) Manoharan, R.; Prabhuram, J. *J. Power Sources* **2001**, *96*, 220. (b) Zhang, X.; Lu, W.; Da, J.; Wang, H.; Zhao, D.; Webley, P. W. *Chem. Commun.* **2009**, 195.

JP9119588